Annals of Diagnostic Pathology 56 (2022) 151871

Contents lists available at ScienceDirect

Annals of Diagnostic Pathology

journal homepage: www.elsevier.com/locate/anndiagpath

Clear cell renal cell carcinoma with prominent microvascular hyperplasia: Morphologic, immunohistochemical and molecular-genetic analysis of 7 sporadic cases

Reza Alaghehbandan [a], Rinë Limani [b], Leila Ali [c], Joanna Rogala [d,e], Tomas Vanecek [d], Petr Steiner [f], Veronika Hajkova [f], Levente Kuthi [g], Maryna Slisarenko [d], Kvetoslava Michalova [d], Kristyna Pivovarcikova [d], Milan Hora [h], Tomas Pitra [h], Michal Michal [d], Ondrej Hes [d,*]

[a] Department of Pathology, Faculty of Medicine, University of British Columbia, Royal Columbian Hospital, Vancouver, BC, Canada
[b] Institute of Pathology, Faculty of Medicine, Hospital and University Clinical Services of Kosovo, Pristina, Kosovo
[c] Department of Pathology, 'Carol Davila' University of Medicine and Pharmacy, Bucharest, Romania
[d] Department of Pathology, Charles University in Prague, Faculty of Medicine in Plzen, Plzen, Czech Republic
[e] Department of Pathology, Regional Specialist Hospital, Wroclaw, Poland
[f] Bioptic Laboratory, Ltd, Molecular Pathology Laboratory, Plzen, Czech Republic
[g] Department of Pathology, University Hospital Szeged, Szeged, Hungary
[h] Department of Urology, Charles University in Prague, Faculty of Medicine in Plzen, Plzen, Czech Republic

ARTICLE INFO

Keywords:
Kidney
Clear cell renal cell carcinoma
Vascular hyperplasia
Microvascular hyperplasia

ABSTRACT

Clear cell renal cell carcinoma (CCRCC) is well known for intratumor heterogeneity. An accurate mapping of the tumor is crucial for assessing prognosis, and perhaps this can be linked to potential success/failure of targeted therapies.

We assembled a cohort of 7 CCRCCs with prominent vasculature and microvascular hyperplasia (ccRCCPV), resembling those seen in high grade gliomas. A control group of classic CCRCC with no variant morphologies was also included. Both groups were analyzed for clinicopathologic, morphologic, immunohistochemical, and molecular genetic features.

No statistically significant differences in mRNA expression of studied genes between the two groups were found. Using NGS panel Trusight Oncology 500 (TSO500), only one clinically significant gene mutation, *VHL* c.263G > A, p. (Trp88Ter), was found. TMB (Tumor Mutation Burden) and MSI (MicroSatellite Instability) were low, and no copy number variations (CNVs) were detected in the study cohort.

Prominent microvascular hyperplasia in CCRCC is a rare phenomenon. From molecular genetic point of view, these tumors do not appear to be different from classic CCRCC. Prognostically, they also demonstrated similar clinical behaviors.

1. Introduction

Clear cell renal cell carcinoma (CCRCC) is the most common renal cell carcinoma, representing approximately 60–70% of all renal cell carcinomas [1,2]. CCRCC is well known for intratumor heterogeneity, which has extensively been studied [2,3].

In the era of personalized (precision) medicine, surgical treatment combined with targeted therapies, such as tyrosine kinase inhibitors, focusing on the tumor neoangiogenesis and driven by *VHL* mutations, generated a glimpse of hope for the treatment of CCRCC. However, this has resulted in partial success so far, mainly due to intratumor heterogeneity [4,5]. Moreover, no systematic genetic testing is usually performed prior to administration of "targeted" therapy with some patients respond very well, while others unfortunately do not and tumors further progress. We believe that an accurate mapping of each tumor is crucial for assessing prognosis and perhaps it can be linked to potential success/failure of a particular targeted therapy.

We assembled a cohort of 7 CCRCCs with prominent vasculature and

* Corresponding author at: Department of Pathology, Charles University, Medical Faculty and Charles University Hospital Plzen, Alej Svobody 80, 304 60 Plzen, Czech Republic.
E-mail address: hes@biopticka.cz (O. Hes).

https://doi.org/10.1016/j.anndiagpath.2021.151871

Available online 25 November 2021

Table 1
Basic clinicopathologic data of CCRCC with prominent vasculature and microvascular hyperplasia.

Case no.	Age (years)	Sex	Size (cm)	TNM UICC 2017	WHO/ISUP Grade	FU (months)
1	71	M	11	pT3a	2	54 AW, AWD[a]
2	51	M	3.1	pT1a	3	39 AW
3	67	F	9	pT3a	2	24 AW
4	78	F	4.4	pT1b	2	40 AW, DUD
5	57	F	6.5	pT3a	2	NA
6	68	M	3.8	pT1a	3	NA
7	70	F	5	pT1b	2	24 AWD[b]

Abbreviations: M male, F female, FU follow up, AW alive and well, AWD alive with disease, DUD death of unrelated disease, NA not available.
[a] Metastases to retroperitoneal lymph nodes and buccal sub-cutis diagnosed 54 months after surgery.
[b] Pulmonary metastases were diagnosed 20 months after nephrectomy, treated by chemotherapy and radiation.

microvascular hyperplasia (ccRCCPV), resembling those seen in high grade gliomas, particularly in glioblastomas. We analyzed these cases according to clinicopathologic, morphologic, immunohistochemical, and molecular genetic features.

2. Material and methods

2.1. Case selection and routine microscopy

Using Plzen Tumor Registry, we selected and reviewed 1268 CCRCCs and subsequently 7 cases were selected and enrolled in the study. The final review and case selection for the study was performed by 3 pathologists (RA, LA, and OH). Clinicopathologic and follow-up data were collected using the available medical records from participating institutions.

The tissue was fixed in 4% formaldehyde, embedded in paraffin using routine procedures. 2 μm thin sections were cut and stained with hematoxylin and eosin. A control group of 5 CCRCCs without prominent vessels were also retrieved from the archive and included in the study. All tumors in the control group were low-stage and low-grade carcinomas. Basic data are available in Supplemental Table.

Non-neoplastic renal parenchymal tissue was available for each examined case (analyzed cases and control group).

2.2. Immunohistochemistry

Immunohistochemical (IHC) stains were performed in one laboratory (University Hospital Plzen), using a Ventana Benchmark XT

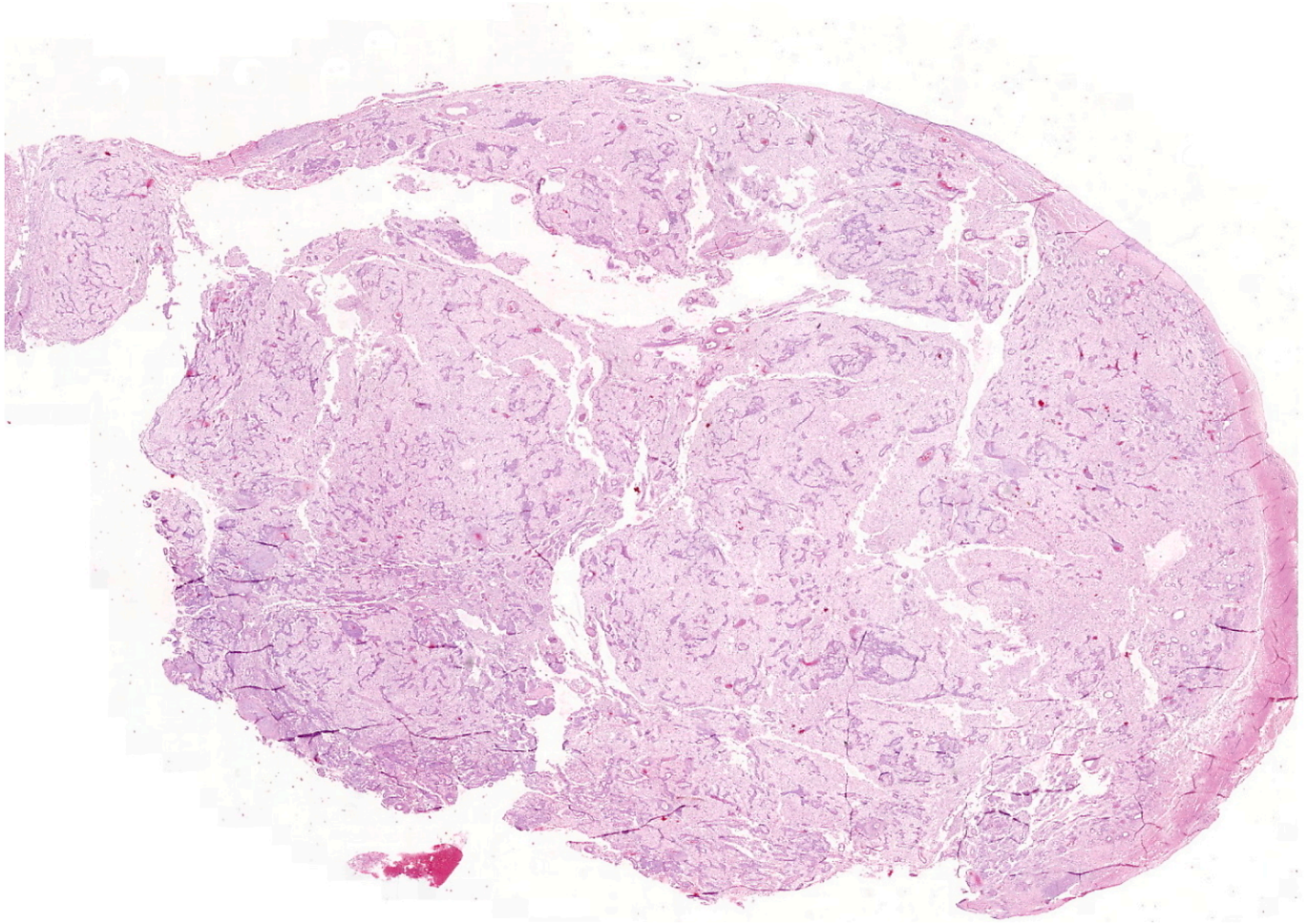

Fig. 1. Solid and alveolar growth patterns in CCRCC with prominent vasculature and microvascular hyperplasia.

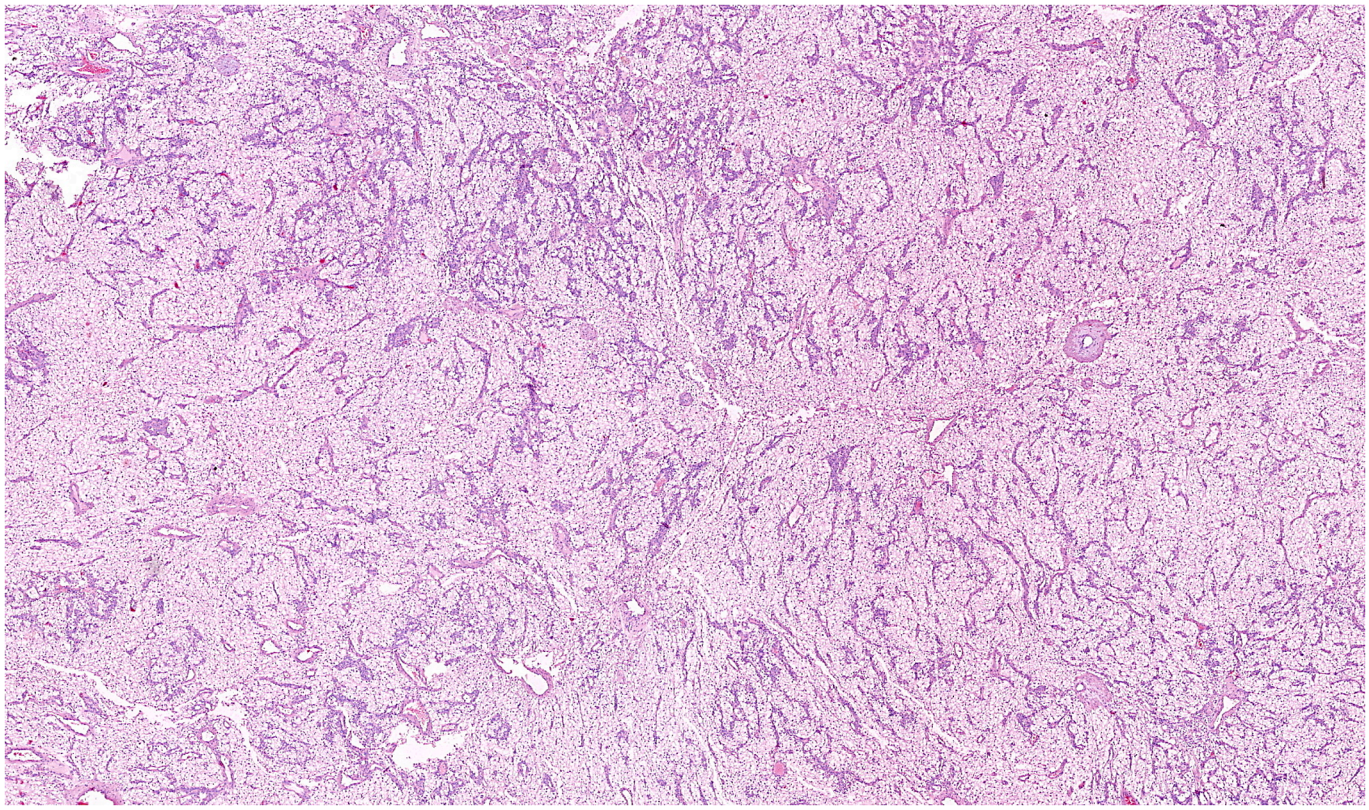

Fig. 2. Prominent vessels in background with thick smooth muscle wall in CCRCC with prominent vasculature and microvascular hyperplasia.

automated stainer (Ventana Medical System, Inc., Tucson, AZ, USA). The following primary antibodies were used: CK7 (OV-TL12/30, monoclonal, Dako, Glostrup, Denmark, 1:200), vimentin (D9, monoclonal, NeoMarkers, Westinghouse, CA, 1:1000), Ki67 (MIB1, monoclonal, Dako, 1:1000), CD31 (JC7OA, monoclonal, Dako, 1:40), and CD34 (QBEnd/10, monoclonal, Dako, 1:200). The primary antibodies were visualized using a supersensitive streptavidin-biotin-peroxidase complex (BioGenex). Internal biotin was blocked by Ventana Benchmark XT automated stainer (hydrogene peroxide based). Appropriate positive and negative controls were also used. The immunohistochemical evaluation was based on the percentage of stained cells (focal positive <50%, diffuse positive >50%, negative 0%).

2.3. Expression analysis

RNA was isolated using a miRNeasy FFPE kit (QIAGEN, Hilden, Germany) according to the manufacturer's instructions. The quantity of isolated RNA was checked on NANODROP 1000 instrument. Five hundred ng of RNA were then reverse-transcribed via RT^2 First Strand Kit (QIAGEN) according to the manufacturer's instructions. As previously described, amplification of 105 and 133 bp product of the *μ2-microglobulin* and 247 bp product of the *PGK* gene was used to test the integrity of extracted RNA [6-8].

Five samples from each group with the best tumor tissue and corresponding non-neoplastic tissue cDNA quality and quantity were subjected to Real-Time RT-PCR analysis performed with RT^2 Profiler PCR Array Human Angiogenesis panel (QIAGEN) according to the manufacturer's instructions, which contains 84 target genes and 5 housekeeping genes.

Relative quantification of target mRNAs in tumor and non-neoplastic tissues was carried out from respective crossing points according to the Livak method [9]. *Beta-2-microglobulin* was used as the best suitable housekeeping gene in this analysis.

Statistical analysis was performed using SAS software (SAS Institute Inc., Cary, NC, USA). Statistical data were measured for parameters in the entire set and in separate groups. Results were also compiled as Box plot graphs. Hypotheses about differential expression of markers between case and control groups were tested using the median pair test. Relative expression differences between the two groups were tested using the exact Wilcoxon test. The statistical significance was set at 5%.

2.4. NGS analysis

Mutation analysis was performed using TruSight Oncology 500 assay (Illumina, San Diego, CA) covering 523 genes (523 for SNVs, 59 for CNVs, 23 for fusions). Complete list of genes in Supplemental Table 2. Total nucleic acid was extracted using FFPE DNA kit (automated on RSC 48 Instrument, Promega, Madison, Wisconsin, USA). Purified nucleic acid was quantified using the Qubit Broad Range DNA/RNA. The quality of DNA was assessed using the FFPE QC kit (Illumina), only DNA samples with Cq <5 were used for further analysis, the quality of RNA using Agilent RNA ScreenTape Assay (Agilent, Santa Clara, CA), only RNA samples with $DV_{200} \geq 20$ were used for further analysis. After DNA enzymatic fragmentation with KAPA FragKit (KAPA Biosystems, Washington, MA), DNA libraries were prepared with the TruSight Oncology 500 assay (Illumina) according to the manufacturer's protocol. Sequencing was performed on the NextSeq 550 sequencer (Illumina) following the manufacturer's recommendations. Data analysis was performed using the local TSO500 analysis software pipeline according to the manufacturer's recommendations. DNA variant filtering and annotation was performed using the OmnomicsNGS analysis software (Euformatics, Finland). Custom variant filter was set up: only non-synonymous variants with coding consequences, read depth greater than 50, gnomAD population frequency less than 0.01, non-benign variants according to the ClinVar database [10]. The remaining filtered variants were checked visually, and sequencing artefacts were excluded.

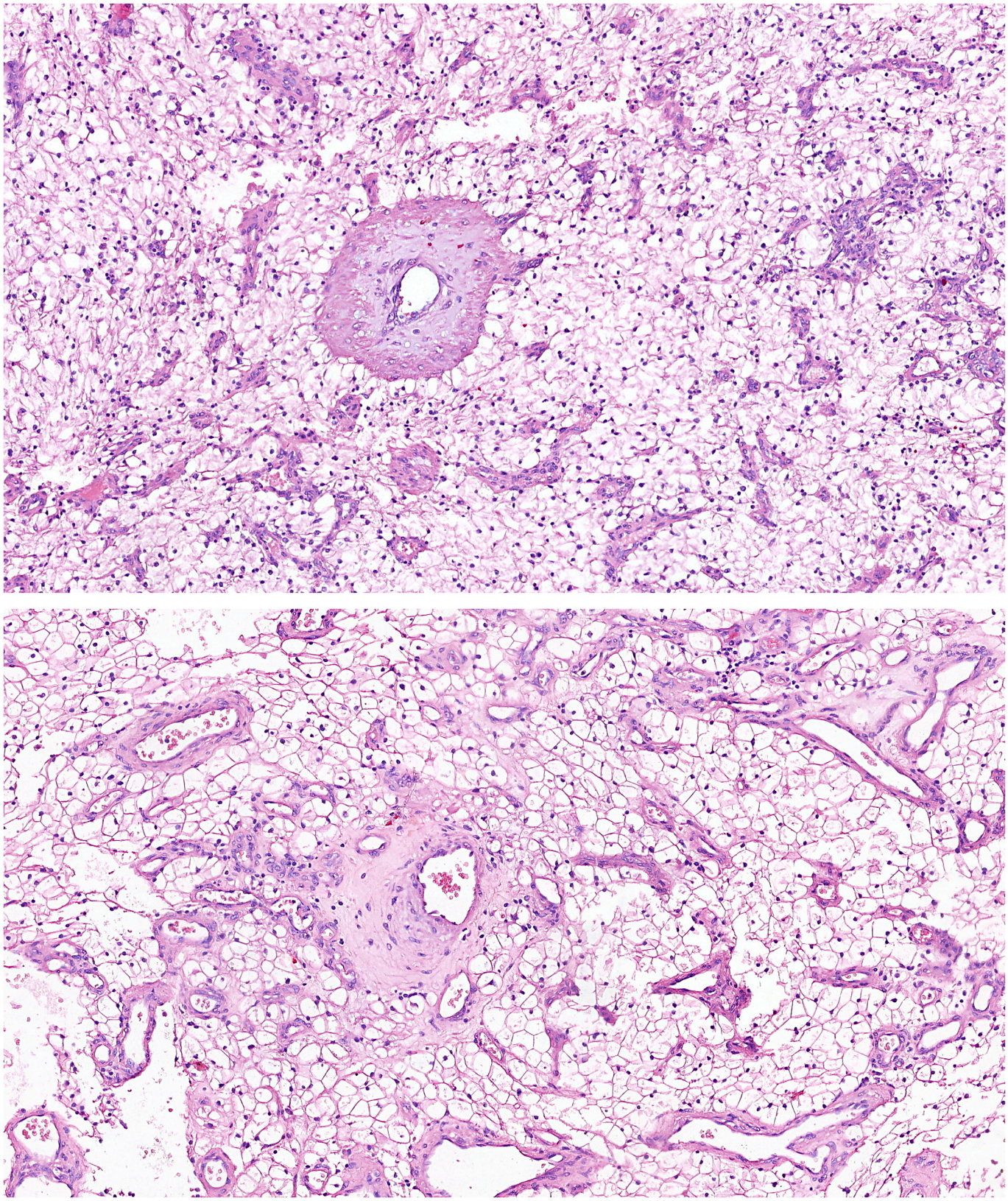

Fig. 3. A and B CCRCC with prominent vasculature and microvascular hyperplasia showing vessels with small caliber forming glomeruloid structures, resembling microvascular hyperplasia in glioblastoma.

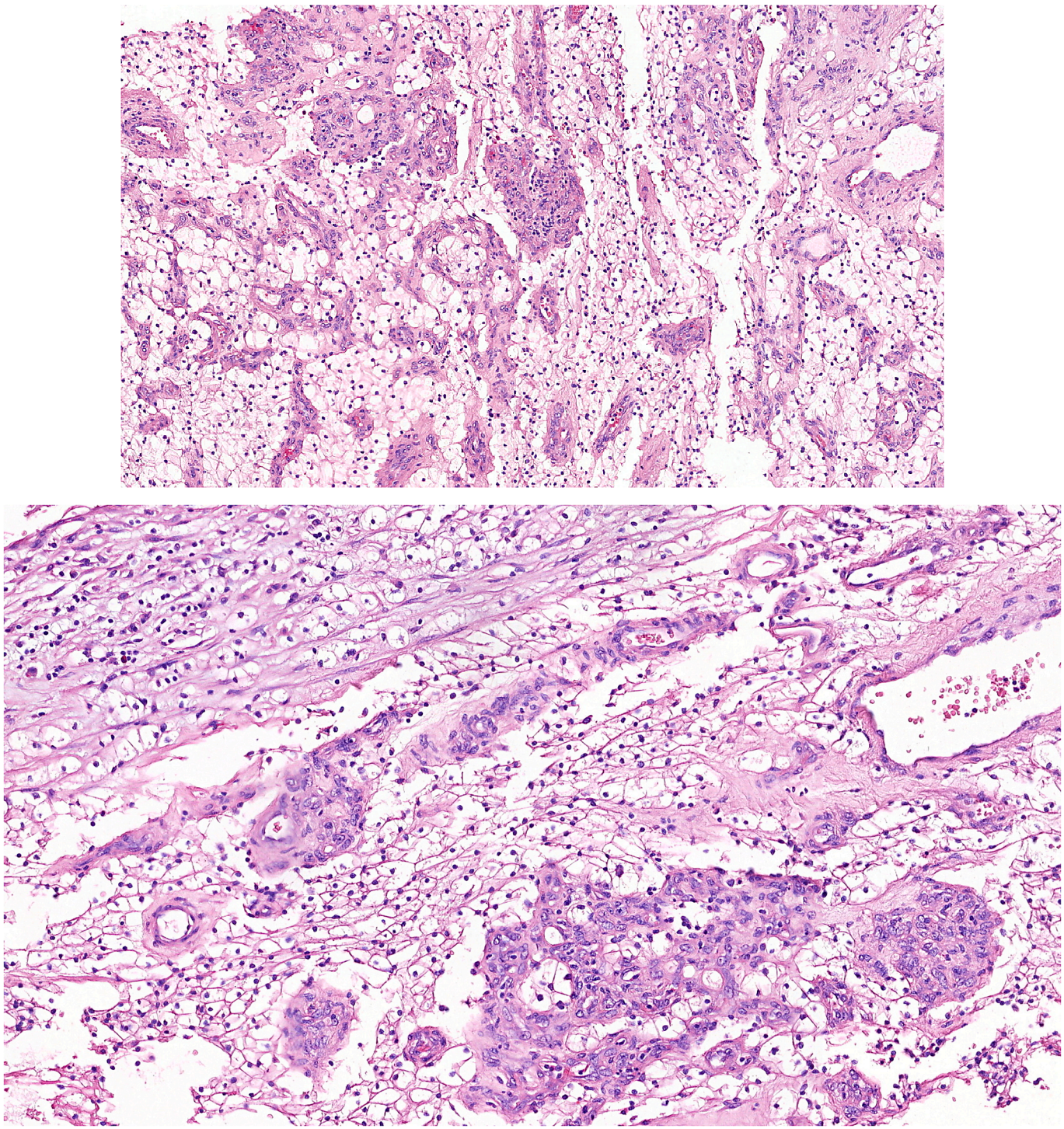

Fig. 4. A–C CCRCC with prominent vasculature and microvascular hyperplasia showing prominent vasculature (thick-walled vessels and glomeruloid formation) diffusely distributed across neoplastic tissue (A). Glomeruloid formations in the vicinity of the abortive vessel (B). The shape of the glomeruloid formations was variable (C).

3. Results

3.1. Clinicopathological data

Basic clinical data on 7 patients with ccRCCPV are presented in Table 1. Patients were 3 males and 4 females, with age range from 51 to 78 years (mean 66, median 68). Tumor size ranged from 3.1 to 11 cm (mean 6.1, median 4.4 cm).

Follow up data were available in 5 patients, ranging from 24 to 54 months (mean 36.2, median 39 months). Aggressive behavior, including metastasis and recurrence, was documented in two cases (cases 1 and 7). In case 1, a metastasis spread to the subcutis of the left buccal area was observed 54 months after the surgery. Subsequently, metastases to retroperitoneal, para-aortic lymph nodes were detected by PET CT. In case 7, two metastases to the lungs were found 20 months post operation. The patient was treated by chemotherapy (cisplatin-based

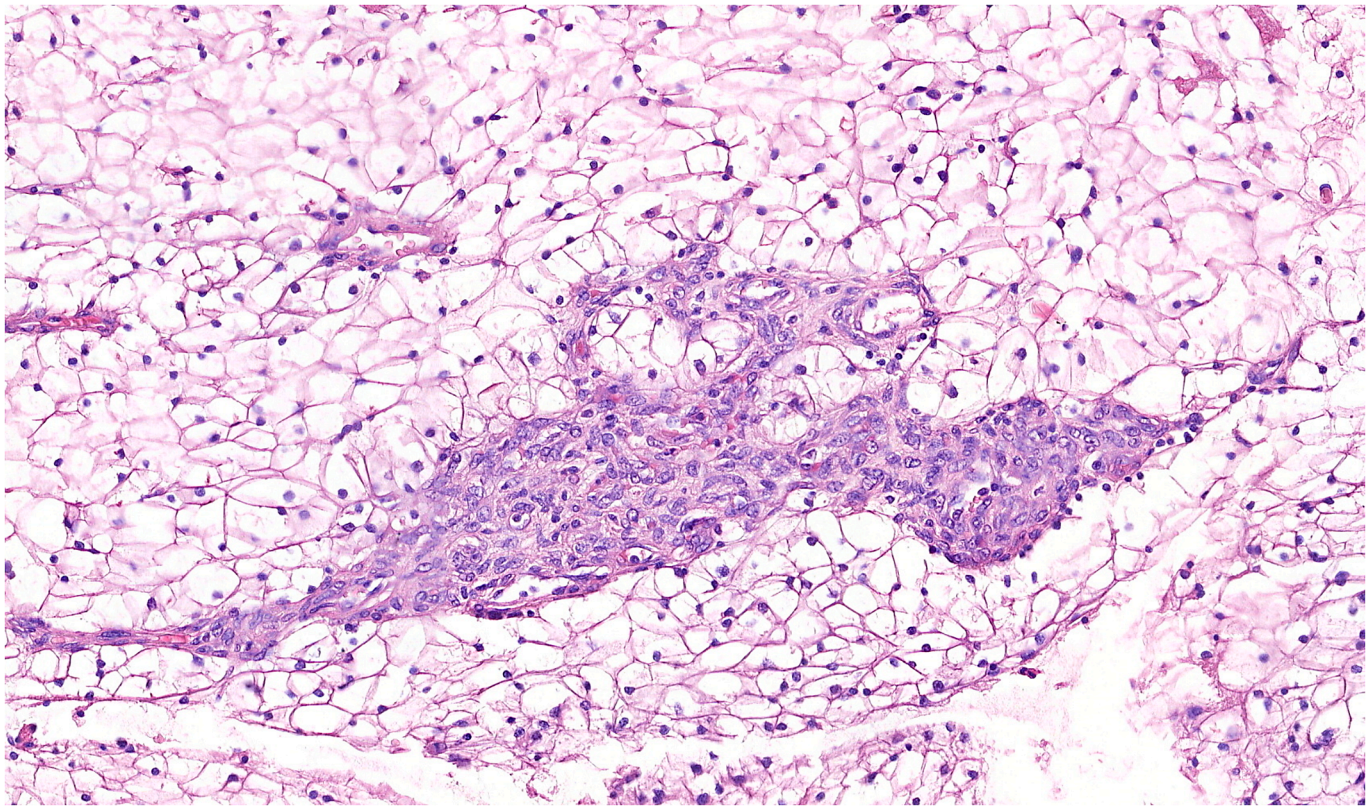

Fig. 4. (*continued*).

Table 2
Results of immunohistochemical analysis of CCRCC with prominent vasculature and microvascular hyperplasia.

Case no.	vim	CANH9	CK7	CD31*	CD34*	Ki67
1	+++	+	−	+++	+++	0–2/hpf
2	+++	++	−	+++	+++	1–5/hpf
3	++	+++	Foc +	+++	+++	0–3/hpf
4	++	+	−	+++	+++	1–5/hpf
5	++	++	−	+++	+++	2–5/hpf
6	+	++	−	+++	+++	2–5/hpf
7	+++	++	Foc +++	+++	+++	10–16/hpf

Abbreviations: + positive, − negative, Foc focally (up to 50% of neoplastic cells), vim vimentin, CANH9 carbonic anhydrase 9,* positive/negative in vessels, hpf high power field.

regiment) and radiotherapy. No progression of the disease was documented two months post chemo-radiation therapy. No signs of von Hippel-Lindau syndrome were found in our patients' family history and medical records.

3.2. Morphologic characteristics

Tumors were all confined to the kidney. Gross sections showed yellow to tan masses, without grossly visible necrotic areas. Small foci of hemorrhage were present. Renal sinus fat invasion was documented in 2 cases (cases 1 and 3).

Tumors were arranged in a solid alveolar pattern, consistent with typical CCRCC morphology (Fig. 1). The neoplastic cells showed voluminous clear cell cytoplasm with mainly WHO/ISUP nuclear grade 2 (focally 3 in some cases). In all seven cases, there were groups of prominent vessels in background with thick smooth muscle wall (Fig. 2). No obvious amorphic depositions such as amyloid, plasmorrhagia or cholesterol clefts were noted. Additionally, vessels with small caliber forming glomeruloid structures, resembling microvascular hyperplasia in glioblastoma, were found (Fig. 3A–B). In four cases, prominent vasculature was present (thick-walled vessels and glomeruloid formation) were present through the whole tumor (Fig. 4A–C). In the remaining three cases, such changes were focally present (less than 30% of total tumorous volume).

3.3. Immunohistochemical examinations

Results of the immunohistochemical examination are presented in Table 2. All cases were positive in the epithelial component for vimentin and CANH9. CK7 was focally positive in 2 cases (case 3 and 7). Prominent thick wall vessels as well as glomeruloid vascular proliferation stained positively for CD31 and CD34 in endothelial cells.

3.4. Molecular genetic findings

The mRNA gene expression in the Angiogenesis panel between the two groups of 5 cases of ccRCCPV and 5 classic CCRCC (as the control group) were compared to their non-neoplastic tissues.

No statistically significant differences were found in mRNA expression between the study groups: ccRCCPV group vs non-neoplastic tissue group (group 1), control group (CCRCC) vs non-neoplastic tissue group (group 2), and group 1 vs group 2 (see Tables 3A, 3B and 3C). No significant differences in expression of examined genes in our cohorts and control group were identified. NGS panel Trusight Oncology 500 (TSO500) demonstrated one pathologically/clinically significant variant, *VHL* c.263G > A, p. (Trp88Ter), AF: 19%, COSM18351, in one of two analyzable samples (case 3) (Table 4). TMB (Tumor Mutation Burden) and MSI (MicroSatellite Instability) were low, and no copy number variations (CNVs) were detected in these 2 cases. Four cases were successfully analyzed in the RNA part, but with no significant findings or fusion transcript was detected. Other samples were not included in the analysis due to suboptimal quality of input material.

Table 3A
Resulting p-values of differences in expression analysis of CCRCC with prominent vasculature and microvascular hyperplasia vs normal tissue cohort.

Gene	p-value	Gene	p-value	Gene	p-value	Gene	p-value
AKT1	0.3750	EGF	0,3750	ITGAV	0,6250	PTGS1	10,000
ANG	0,1250	ENG	0,3750	ITGB3	0,0625	S1PR1	0,6250
ANGPT1	0,3750	EPHB4	0,3750	JAG1	0,3750	SERPINE1	10,000
ANGPT2	10,000	ERBB2	10,000	KDR	0,3750	SERPINF1	0,3750
ANGPTL4	10,000	F3	N/A	LECT1	10,000	SPHK1	0,1250
ANPEP	0,3750	FGF1	0,2500	LEP	0,3750	TEK	10,000
ADGRB1	0,1250	FGF2	0,1250	MDK	0,5000	TGFA	0,0625
CCL11	0,0625	FGFR3	0,0625	MMP14	10,000	TGFB1	0,3750
CCL2	10,000	FIGF	0,3750	MMP2	0,3750	TGFB2	0,6250
CDH5	0,0625	FLT1	0,1250	MMP9	0,3750	TGFBR1	0,3750
COL18A1	0,3750	FN1	0,3750	NOS3	10,000	THBS1	0,3750
COL4A3	0,3750	HGF	0,6250	NOTCH4	10,000	THBS2	10,000
CTGF	0,0625	HIF1A	10,000	NRP1	0,3750	TIE1	0,3750
CXCL1	10,000	HPSE	0,3750	NRP2	10,000	TIMP1	0,3750
CXCL10	0,6250	ID1	10,000	PDGFA	0,0625	TIMP2	0,3750
CXCL5	10,000	IFNA1	10,000	PECAM1	0,3750	TIMP3	0,0625
CXCL6	N/A	IFNG	10,000	PF4	0,6250	TNF	10,000
CXCL9	0,3750	IGF1	10,000	PGF	0,0625	TYMP	0,3750
EDN1	10,000	IL1B	10,000	PLAU	0,3750	VEGFA	0,0625
EFNA1	0,0625	IL6	10,000	PLG	0,2500	VEGFB	0,0625
EFNB2	0,3750	CXCL8	0,3750	PROK2	10,000	VEGFC	0,6250

Abbreviations: N/A: not analyzable.

Table 3B
Resulting p-values of differences in expression analysis of control tumors vs normal tissue cohort.

Gene	p-value	Gene	p-value	Gene	p-value	Gene	p-value
AKT1	0,2500	EGF	0,3750	ITGAV	10,000	PTGS1	0,6250
ANG	0,0625	ENG	0,6250	ITGB3	0,0625	S1PR1	0,6250
ANGPT1	0,0625	EPHB4	0,3750	JAG1	10,000	SERPINE1	10,000
ANGPT2	10,000	ERBB2	0,0625	KDR	0,3750	SERPINF1	0,3750
ANGPTL4	0,3750	F3	10,000	LECT1	N/A	SPHK1	0,1250
ANPEP	0,0625	FGF1	10,000	LEP	0,0625	TEK	0,5000
ADGRB1	0,0625	FGF2	0,3750	MDK	0,6250	TGFA	0,3750
CCL11	10,000	FGFR3	0,0625	MMP14	0,3750	TGFB1	10,000
CCL2	0,2500	FIGF	0,0625	MMP2	0,3750	TGFB2	10,000
CDH5	10,000	FLT1	0,1250	MMP9	10,000	TGFBR1	0,3750
COL18A1	0,0625	FN1	0,0625	NOS3	0,3750	THBS1	0,3750
COL4A3	0,0625	HGF	0,3750	NOTCH4	0,6250	THBS2	0,5000
CTGF	0,0625	HIF1A	10,000	NRP1	10,000	TIE1	0,3750
CXCL1	0,2500	HPSE	0,0625	NRP2	10,000	TIMP1	10,000
CXCL10	10,000	ID1	0,0625	PDGFA	0,3750	TIMP2	0,0625
CXCL5	0,0625	IFNA1	10,000	PECAM1	0,3750	TIMP3	0,0625
CXCL6	10,000	IFNG	0,1250	PF4	0,6250	TNF	0,3750
CXCL9	10,000	IGF1	10,000	PGF	0,1250	TYMP	10,000
EDN1	10,000	IL1B	10,000	PLAU	0,0625	VEGFA	0,3750
EFNA1	0,3750	IL6	10,000	PLG	0,1250	VEGFB	0,3750
EFNB2	0,3750	CXCL8	10,000	PROK2	0,3750	VEGFC	10,000

Abbreviations: N/A: not analyzable.

4. Discussion

According to the 2016 WHO Classification and the 8th AJCC Cancer Staging Manual, the most important prognostic parameter for RCC is the TNM stage. CCRCC is no exception; however, further prognostic parameters such as histologic grade, tumor necrosis, and sarcomatoid/rhabdoid differentiation are also established [1,11,12].

The vast majority of CCRCCs are easily diagnosed based on H&E histologic sections, including their adverse prognostic features. Over the last few decades, the spectrum of CCRCC morphologic variants has evolved beyond the classic low-grade CCRCC and the high-grade counterpart with larger, mostly eosinophilic cells (so-called "granular" variant) [12-19].

The architecture of CCRCC is usually alveolar, however tubular, pseudopapillary or even true papillary patterns have also been documented [1,19]. Further, CCRCC with mucin production, CCRCC with syncytial trophoblastic cell-like proliferation, CCRCC with extramedullary megakaryopoiesis and other morphologic variants have been described [14,15,19,20].

Tumor heterogeneity might be one of the many potential reasons, why some tumors are resistant to the treatment. Although it would be possible to sample tumor extensively, genetic testing is not widely used before administration of any targeted/biologic therapy in RCCs [21-23]. CCRCC harbors an abundant vasculature resulted from the pseudohypoxic microenvironment due to the *VHL* inactivation. Those vessels are responsible for the tumor progression and treatment failure. High expression of genes involved in the HIF-VEGF-VEGFR-pro-angiogenic pathway has been documented and associated with better response to targeted therapy [24-26]. In fact, antiangiogenic VEGF-TKIs, such as sunitinib, are currently used as the first-line treatments in CCRCC.

In this study, we selectively chose a set of CCRCCs with commonly shared features. They were all low-grade tumors, with alveolar growth pattern and classic morphology (no architectural or morphologic variants included). Additionally, they showed two types of unusual vascular proliferation (unlike typical rich delicate capillary vasculature). First, thick-walled hypercellular vessels were haphazardly present across the

Table 3C
Resulting p-values of differences in expression analysis of CCRCC with prominent vasculature and microvascular hyperplasia vs control tumors vs normal tissue cohort.

Gene	p-value	Gene	p-value	Gene	p-value	Gene	p-value
AKT1	10,000	EGF	0,8413	ITGAV	0,7302	PTGS1	0,7302
ANG	0,5556	ENG	0,2857	ITGB3	0,4206	S1PR1	0,8857
ANGPT1	0,2222	EPHB4	0,0952	JAG1	0,5476	SERPINE1	0,6905
ANGPT2	0,4206	ERBB2	0,4206	KDR	0,4206	SERPINF1	10,000
ANGPTL4	0,1508	F3	N/A	LECT1	N/A	SPHK1	0,4857
ANPEP	0,5476	FGF1	0,4000	LEP	0,1508	TEK	0,6667
ADGRB1	0,2857	FGF2	0,1905	MDK	0,8000	TGFA	0,1508
CCL11	0,6905	FGFR3	0,8413	MMP14	10,000	TGFB1	0,0952
CCL2	0,2500	FIGF	0,5476	MMP2	10,000	TGFB2	0,2857
CDH5	0,3095	FLT1	0,3429	MMP9	0,0952	TGFBR1	0,5476
COL18A1	0,4206	FN1	0,1508	NOS3	0,9048	THBS1	0,6905
COL4A3	0,2222	HGF	0,4127	NOTCH4	0,5556	THBS2	10,000
CTGF	0,2222	HIF1A	0,5476	NRP1	0,3095	TIE1	0,3095
CXCL1	0,4000	HPSE	0,8413	NRP2	10,000	TIMP1	0,8413
CXCL10	0,8571	ID1	0,4127	PDGFA	0,4206	TIMP2	0,4206
CXCL5	0,6905	IFNA1	10,000	PECAM1	0,0952	TIMP3	10,000
CXCL6	N/A	IFNG	0,1111	PF4	0,3429	TNF	0,7857
CXCL9	0,6905	IGF1	0,4000	PGF	0,7302	TYMP	0,8413
EDN1	0,8413	IL1B	10,000	PLAU	0,5476	VEGFA	0,8413
EFNA1	0,1508	IL6	0,8413	PLG	0,8571	VEGFB	0,1508
EFNB2	0,3095	CXCL8	0,0952	PROK2	0,4206	VEGFC	0,5556

Abbreviations: N/A: not analyzable.

Table 4
Results of NGS TSO 500 analysis of CCRCC with prominent vasculature and microvascular hyperplasia.

Case	Age	Sex	QC	TS500D	Variants	TMB	CNV	MSI	TS500R
1	71	M	PASS	FAIL					neg
2	51	M	FAIL	ND					ND
3	67	F	PASS	PASS	VHL c.263G > A, p.(Trp88Ter), AF: 19%, COSM18351	Low (8,7mut/Mb)	neg	Low (4,8% loci)	neg
4	78	F	PASS	FAIL					neg
5	57	F	PASS	PASS	neg	Low (3,9mut/Mb)	neg	Low (2,9% loci)	neg
6	68	M	FAIL	ND					ND
7	70	F	FAIL	ND					ND

Abbreviations: QC Quality Control, M male, F female, TS500D DNA part, TS500R RNA part, TMB Tumor Mutation Burden, CNV Copy Number Variation, MSI Microsatellite Instability, ND not done, NEG negative.

tumorous mass. In cases, where vessels were present mostly focally, they were easy to identify at scanning magnification. The second unusual vascular structures were those with small caliber (larger than capillaries) and forming glomeruloid formations. Similar vascular proliferation is known in extra-renal tumors, such as high -grade astrocytomas/gliomas [27,28]. Such vessel formation is denominated as microvascular proliferation. Within glial tumors, the presence of such vessels usually is one of the diagnostic features of high-grade glial tumor. The presence of unusual vascular glomeruloid formations and thick-walled vessels in this cohort do not appear to play a significant prognostic role. Also, this phenomenon should be interpreted with caution given our small sample size and relatively short clinical follow-up period.

In order to assess the significance of unusual vasculature in CCRCC, we compared CCRCCs with glioblastoma-like vessels to a control group of classic CCRCCs without glioblastoma-like vessels. We found no statistically significant differences in studied angiogenesis-related genes between the two cohorts.

In our study, we attempted to find genes responsible for rich vascular proliferation. Using panel with 500 genes, except for one mutation of the *VHL* gene (*VHL* c.263G > A, p. (Trp88Ter)), no other genetic changes associated with vascular proliferation were identified. Thus, it may be possible that the presence of prominent vasculature in these tumors could be caused by other genes not included in our panel. It should also be noted that not all cases in this study were analyzable genetically.

The presence of glioblastoma-like vessels in CCRCC seems to be a somewhat rare finding, with a rate of less than 1% based on our study population. Nonetheless, it can present a potential challenge in the differential diagnostic workup, particularly in small sample. A few renal neoplasms may present with such vascular features as epithelioid angiomyolipoma (AML), t6;11 translocation RCC, SDH deficient RCCs, and eosinophilic vacuolated tumor (EVT).

Epithelioid AML is a rare variant of AML with predominant epithelioid histology (carcinoma-like) and prominent thick-walled vessels. However, in AML vessels can be very prominent and usually distorted, and the neoplastic cells mostly lack clear cytoplasm. There can also be more typical histologic features such as smooth muscle and/or adipocytic proliferation. In doubtful cases, immunohistochemical examination with HMB45 and Melan-A can help to reach the correct diagnosis [29].

t(6;11) translocation RCC is another tumor with thick-walled vessels; however they are not as prominent as seen in AML and can be absent in some cases. In typical t(6;11) translocation RCC, nests of rosettes clustered around the basement membrane combined with large eosinophilic cells are, together with immunohistochemical profile (positivity with melanocytic markers and *TFEB* gene break) diagnostic [30].

The other renal tumors that can have aberrant vessels are SDH-deficient RCCs and eosinophilic vacuolated tumor (EVT). In both tumors, the vessels lack hypercellular appearance, which is seen in CCRCC with glioblastoma-like vessels and also lack microvascular hyperplasia [31,32]. Further, architecture and cytologic features are far from the clear cell population documented in cases from our series.

5. Conclusions

Prominent microvascular hyperplasia in CCRCC is a rare phenomenon. From the molecular genetic point of view, these tumors do not appear to be different from classic CCRCC. Prognostically, they also demonstrated similar clinical behaviors. Our study findings further

enhance our understanding of intratumor heterogeneity in CCRCC.

Funding

The study was supported in part by the Charles University Research Fund (project number Q39), the project Institutional Research Fund of University Hospital Plzen (Faculty Hospital in Plzen- FNPl 00669806), and grant Charles University Fund SVV-2020-2022 260539.

Declaration of competing interest

The authors have no conflicts of interest to declare that are relevant to the content of this article.

Appendix A. Supplementary data

Supplementary data to this article can be found online at https://doi.org/10.1016/j.anndiagpath.2021.151871.

References

[1] Moch H, Humphrey PA, Ulbricht TM, Reuter W. IARC Lyon. 2016. p. 18–21.
[2] Trpkov K, Williamson SR, Gill AJ, Adeniran AJ, Agaimy A, Alaghehbandan R, et al. Novel, emerging and provisional renal entities: the genitourinary pathology society (GUPS) update on renal neoplasia. Mod Pathol 2021;34(6):1167–84.
[3] Cortes JM, de Petris G, Lopez JI. Detection of intratumor heterogeneity in modern pathology: a multisite tumor sampling perspective. Front Med (Lausanne) 2017;4:25.
[4] Pichler R, Heidegger I. Novel concepts of antiangiogenic therapies in metastatic renal cell cancer. Memo. 2017;10(4):206–12.
[5] Lee CH, Motzer RJ. Kidney cancer in 2016: the evolution of anti-angiogenic therapy for kidney cancer. Nat Rev Nephrol 2017;13(2):69–70.
[6] Antonescu CR, Kawai A, Leung DH, Lonardo F, Woodruff JM, Healey JH, et al. Strong association of SYT-SSX fusion type and morphologic epithelial differentiation in synovial sarcoma. Diagn Mol Pathol 2000;9(1):1–8.
[7] Gaffney R, Chakerian A, O'Connell JX, Mathers J, Garner K, Joste N, et al. Novel fluorescent ligase detection reaction and flow cytometric analysis of SYT-SSX fusions in synovial sarcoma. J Mol Diagn 2003;5(2):127–35.
[8] Viswanatha DS, Foucar K, Berry BR, Gascoyne RD, Evans HL, Leith CP. Blastic mantle cell leukemia: an unusual presentation of blastic mantle cell lymphoma. Mod Pathol 2000;13(7):825–33.
[9] Livak KJ, Schmittgen TD. Analysis of relative gene expression data using real-time quantitative PCR and the 2(-Delta Delta C(T)) method. Methods. 2001;25(4):402–8.
[10] Landrum MJ, Lee JM, Benson M, Brown GR, Chao C, Chitipiralla S, et al. ClinVar: improving access to variant interpretations and supporting evidence. Nucleic Acids Res 2018;46(D1):D1062–7.
[11] Delahunt B, McKenney JK, Lohse CM, Leibovich BC, Thompson RH, Boorjian SA, et al. A novel grading system for clear cell renal cell carcinoma incorporating tumor necrosis. Am J Surg Pathol 2013;37(3):311–22.
[12] de Peralta-Venturina M, Moch H, Amin M, Tamboli P, Hailemariam S, Mihatsch M, et al. Sarcomatoid differentiation in renal cell carcinoma: a study of 101 cases. Am J Surg Pathol 2001;25(3):275–84.
[13] Rotterova P, Martinek P, Alaghehbandan R, Prochazkova K, Damjanov I, Rogala J, et al. High-grade renal cell carcinoma with emperipolesis: Clinicopathological, immunohistochemical and molecular-genetic analysis of 14 cases. Histol Histopathol 2018;33(3):277–87.
[14] Williamson SR, Mast KJ, Cheng L, Idrees MT. Clear cell renal cell carcinoma with intratumoral and nodal extramedullary megakaryopoiesis: a potential diagnostic pitfall. Hum Pathol 2014;45(6):1306–9.
[15] Williamson SR, Kum JB, Goheen MP, Cheng L, Grignon DJ, Idrees MT. Clear cell renal cell carcinoma with a syncytial-type multinucleated giant tumor cell component: implications for differential diagnosis. Hum Pathol 2014;45(4):735–44.
[16] Tanas Isikci O, He H, Grossmann P, Alaghehbandan R, Ulamec M, Michalova K, et al. Low-grade spindle cell proliferation in clear cell renal cell carcinoma is unlikely to be an initial step in sarcomatoid differentiation. Histopathology. 2018;72(5):804–13.
[17] Rogala J, Kojima F, Alaghehbandan R, Agaimy A, Martinek P, Ondic O, et al. Papillary renal cell carcinoma with prominent spindle cell stroma - tumor mimicking mixed epithelial and stromal tumor of the kidney: Clinicopathologic, morphologic, immunohistochemical and molecular genetic analysis of 6 cases. Ann Diagn Pathol 2020;44:151441.
[18] Petersson F, Martinek P, Vanecek T, Pivovarcikova K, Peckova K, Ondic O, et al. Renal cell carcinoma with leiomyomatous stroma: a Group of Tumors with indistinguishable histopathologic features, but 2 distinct genetic profiles: next-generation sequencing analysis of 6 cases negative for aberrations related to the VHL gene. Appl Immunohistochem Mol Morphol 2018;26(3):192–7.
[19] Alaghehbandan R, Ulamec M, Martinek P, Pivovarcikova K, Michalova K, Skenderi F, et al. Papillary pattern in clear cell renal cell carcinoma: clinicopathologic, morphologic, immunohistochemical and molecular genetic analysis of 23 cases. Ann Diagn Pathol 2019;38:80–6.
[20] Val-Bernal JF, Salcedo W, Val D, Parra A, Garijo MF. Mucin-secreting clear cell renal cell carcinoma. A rare variant of conventional renal cell carcinoma. Ann Diagn Pathol 2013;17(2):226–9.
[21] Makhov P, Joshi S, Ghatalia P, Kutikov A, Uzzo RG, Kolenko VM. Resistance to systemic therapies in clear cell renal cell carcinoma: mechanisms and management strategies. Mol Cancer Ther 2018;17(7):1355–64.
[22] Lopez JI, Cortes JM. Multisite tumor sampling: a new tumor selection method to enhance intratumor heterogeneity detection. Hum Pathol 2017;64:1–6.
[23] Guarch R, Lawrie CH, Larrinaga G, Angulo JC, Pulido R, Lopez JI. High levels of intratumor heterogeneity characterize the expression of epithelial-mesenchymal transition markers in high-grade clear cell renal cell carcinoma. Ann Diagn Pathol 2018;34:27–30.
[24] Beuselinck B, Verbiest A, Couchy G, Job S, de Reynies A, Meiller C, et al. Pro-angiogenic gene expression is associated with better outcome on sunitinib in metastatic clear-cell renal cell carcinoma. Acta Oncol 2018;57(4):498–508.
[25] Mikami S, Mizuno R, Kosaka T, Tanaka N, Kuroda N, Nagashima Y, et al. Significance of tumor microenvironment in acquiring resistance to vascular endothelial growth factor-tyrosine kinase inhibitor and recent advance of systemic treatment of clear cell renal cell carcinoma. Pathol Int 2020;70(10):712–23.
[26] Sharma R, Kadife E, Myers M, Kannourakis G, Prithviraj P, Ahmed N. Determinants of resistance to VEGF-TKI and immune checkpoint inhibitors in metastatic renal cell carcinoma. J Exp Clin Cancer Res 2021;40(1):186.
[27] Wesseling P, Schlingemann RO, Rietveld FJ, Link M, Burger PC, Ruiter DJ. Early and extensive contribution of pericytes/vascular smooth muscle cells to microvascular proliferation in glioblastoma multiforme: an immuno-light and immuno-electron microscopic study. J Neuropathol Exp Neurol 1995;54(3):304–10.
[28] Haddad SF, Moore SA, Schelper RL, Goeken JA. Vascular smooth muscle hyperplasia underlies the formation of glomeruloid vascular structures of glioblastoma multiforme. J Neuropathol Exp Neurol 1992;51(5):488–92.
[29] Calio A, Brunelli M, Segala D, Zamboni G, Bonetti F, Pea M, et al. Angiomyolipoma of the kidney: from simple hamartoma to complex tumour. Pathology. 2021;53(1):129–40.
[30] Argani P, Yonescu R, Morsberger L, Morris K, Netto GJ, Smith N, et al. Molecular confirmation of t(6;11)(p21;q12) renal cell carcinoma in archival paraffin-embedded material using a break-apart TFEB FISH assay expands its clinicopathologic spectrum. Am J Surg Pathol 2012;36(10):1516–26.
[31] He H, Trpkov K, Martinek P, Isikci OT, Maggi-Galuzzi C, Alaghehbandan R, et al. "high-grade oncocytic renal tumor": morphologic, immunohistochemical, and molecular genetic study of 14 cases. Virchows Arch 2018;473(6):725–38.
[32] Gill AJ, Hes O, Papathomas T, Sedivcova M, Tan PH, Agaimy A, et al. Succinate dehydrogenase (SDH)-deficient renal carcinoma: a morphologically distinct entity: a clinicopathologic series of 36 tumors from 27 patients. Am J Surg Pathol 2014;38(12):1588–602.